NANO LETTERS
Cite This: Nano Lett. 2019, 19, 5829−5835
Letter
pubs.acs.org/NanoLett

Direct Writing of Tunable Living Inks for Bioprocess Intensification

Fang Qian,*,† Cheng Zhu,‡ Jennifer M. Knipe,† Samantha Ruelas,† Joshuah K. Stolaroff,§ Joshua R. DeOtte,‡,⊥ Eric B. Duoss,‡ Christopher M. Spadaccini,‡ Calvin A. Henard,¶ Michael T. Guarnieri,¶ and Sarah E. Baker*,†

†Physical and Life Science Directorate, ‡Engineering Directorate, and §Global Security, Lawrence Livermore National Laboratory, Livermore, California 94550, United States

⊥University of California, Davis, California 95616, United States

¶National Bioenergy Center, National Renewable Energy Laboratory, Golden, Colorado 80401, United States

Supporting Information

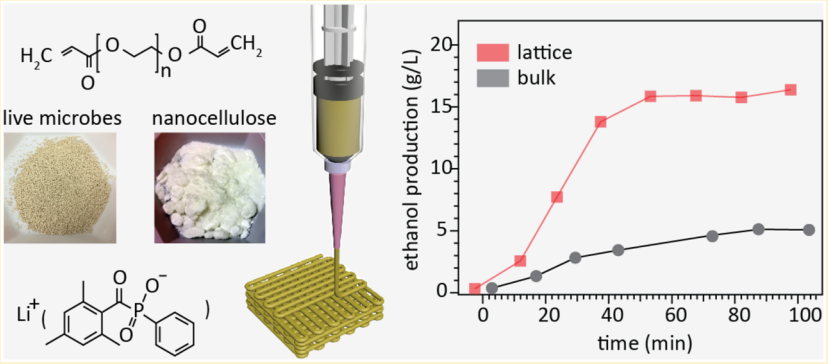

ABSTRACT: Critical to the success of three-dimensional (3D) printing of living materials with high performance is the development of new ink materials and 3D geometries that favor long-term cell functionality. Here we report the use of freeze-dried live cells as the solid filler to enable a new living material system for direct ink writing of catalytically active microorganisms with tunable densities and various self-supporting porous 3D geometries. Baker's yeast was used as an exemplary live whole-cell biocatalyst, and the printed structures displayed high resolution, large scale, high catalytic activity and long-term viability. An unprecedented high cell loading was achieved, and cell inks showed unique thixotropic behavior. In the presence of glucose, printed bioscaffolds exhibited increased ethanol production compared to bulk counterparts due largely to improved mass transfer through engineered porous structures. The new living materials developed in this work could serve as a versatile platform for process intensification of an array of bioconversion processes utilizing diverse microbial biocatalysts for production of high-value products or bioremediation applications.

KEYWORDS: *Bioprinting, bioinks, living materials, biocatalysts, additive manufacturing*

Bioprinting is a powerful technology to create complex 3D scaffolds that contain living cells and has been demonstrated for applications ranging from biosensing to tissue regeneration, environment sensing, drug discovery, and clinical implementation.[1] The key to the success of bioprinting applications is the development of ink materials, or a "bio-inks", which integrate live cells with supporting hydrogels into a printable ink that can be further fabricated into customized 3D geometries. In the past few years, bioprinting research has made tremendous achievements, especially on printing mammalian cells, tissues, and organs.[2−7]

In addition to mammalian cells, there is a growing interest in the bioprinting of functional microbes as biocatalysts. Microbes are extensively used in industry to convert carbon sources into valuable end-product chemicals and have found applications in the food industry, biofuel production, waste treatment, and bioremediation.[8] Using live microbes versus inorganic catalysts has advantages of mild reaction conditions, self-regeneration, low cost, and catalytic specificity.[8,9] Lehner et al. used alginate as the hydrogel base and printed multifluorescent *E. coli* strains.[10] Later on, Schaffner et al. reported an ultraviolent (UV)-curable, multicomponent ink containing *P. putida* or *B. subtilis*, and both exhibited an active metabolism.[11] Liu et al. reported another UV-curable bioink fomula that immobilized engineered *E. coli* strain for use as multipurpose chemical sensors.[12] More recently, Saha et al. reported printed *Saccharomyces cerevisiae* strain SO992 scaffold for glucose fermentation.[13] In these previous studies, a diluted cell suspension was added to a hydrogel already optimized for extrusion-based printing. These bioinks had low cell concentration that may limit the volumetric productivity in

Received: January 7, 2019
Published: January 31, 2019

DOI: 10.1021/acs.nanolett.9b00066
Nano Lett. 2019, 19, 5829−5835

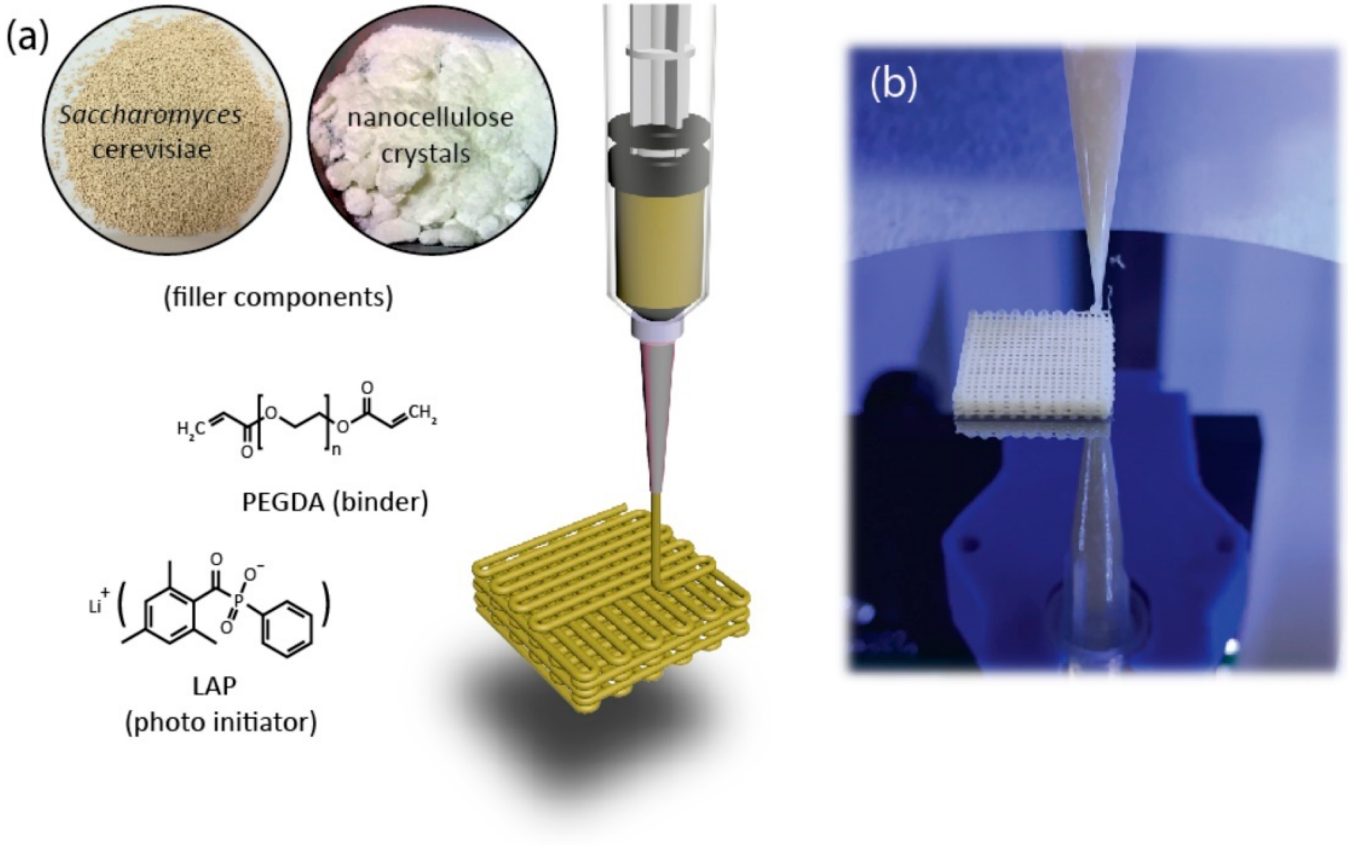

Figure 1. Preparation and printing of bioinks with tunable cell loading. (a) Schematic of the ink components of filler(s), binder, and photoinitiator. (b) Photograph of the printing nozzle in the process of writing a 3D scaffold structure.

biocatalysis. In addition, while the biocompatibility of hydrogels is extensively studied, the impact of cells on ink properties has not been reported because the effect of cells is negligible when cell loading is low.

In this work, we demonstrated a new bioink system and printed catalytically active live cells into various self-supporting 3D geometries with fine filament thicknesses (down to 100 μm), large scale (up to 225 cm^2), tunable cell densities, and high catalytic productivity. Baker's yeast (*Saccharomyces cerevisiae*) was employed as an exemplary biocatalyst for glucose fermentation. Unlike previous work, our ink employed freeze-dried cells and thus achieved an extremely high cell loading up to 42.8 wt % (or 75 vol %). At such high loading, we discovered a new phenomenon that the cells alone can function as a viscosifier to yield a unique shear-thinning ink, and the physical properties of the ink became dictated by the physical properties of the cells. Adding nanocellulose as an optional secondary filler assisted the control of intercellular distance. In the presence of glucose, printed cells produce ethanol and carbon dioxide gas (CO_2) with a short lag period, as confirmed by immediate gas bubble generation and quantitative ethanol assay. Printed scaffolds exhibited enhanced activity relative to bulk counterparts, which indicated that mass transfer limit at high cell densities could be ameliorated by macroporous structures. Printed cells were metabolically active up to 4 months and redistributed themselves via local proliferation. Additive manufacturing of live whole-cells can serve as a versatile platform for fundamental studies of microbial behaviors, communications, and interaction with the microenvironment, and for new bioreactors with high volumetric productivity and long lifetime.

A scheme for ink preparation and real-time printing is shown in Figure 1 and Video 1. Used alone, freeze-dried yeast cells functioned as an excellent viscosifier and above a certain loading (~30 wt %) yielded a printable ink. Similarly, nanocellulose can also generate shear-thinning inks. Scanning electron microscope (SEM) images showed as-received yeast granules consisted of closely packed cells, while nanocellulose powder had nanofibrous structures (Figure S1). Fillers were mixed in sterile phosphate-buffered saline solution containing 10 wt % of polyethylene glycol dimethacrylate (PEGDA, MW 20000) and 0.01 wt % of lithium phenyl-2,4,6-trimethylbenzoylphosphinate (LAP). The usage of LAP as a photoinitiator allows photocuring at a wavelength of 405 nm and may cause less UV damage to the cells compared to Irgacure (used at 365 nm wavelength).[14] All these components were mixed well until a dough-like ink was formed. The inks can be readily loaded into a syringe barrel and then extruded through a nozzle to print programmed 3D structures, which are then photocured and soaked in yeast peptone dextrose (YPD) medium containing 2 wt % glucose.

Yeast granules and nanocellulose can also be used in combination with almost arbitrary ratios. These dual-filler formula allows comprehensive control of ink rheology and cell density over a wide range. Figure 2a shows the formula of five representative inks with systematically increased yeast-to-nanocellulose weight ratio (Y/N ratio) from 0 to 1, with cell loading from 0% to 42.8 wt %. Given each gram of Baker's yeast contains 20 billion cells,[15] the cell density of ink #5 (pure

DOI: 10.1021/acs.nanolett.9b00066
Nano Lett. 2019, 19, 5829−5835

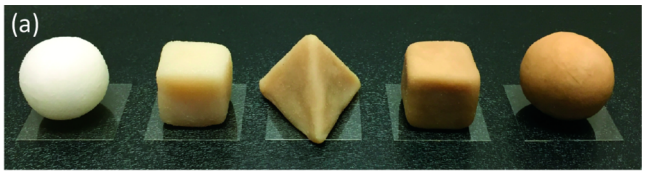

	Ink #1 (cellulose ink)	Ink #2	Ink #3	Ink #4	Ink #5 (yeast ink)
Yeast (Y)	n/a	0.6 g	1.3 g	2.8 g	30 g
Nanocellulose (N)	36 g	34.4 g	33.2 g	28.0 g	n/a
PBS	36 g	36 g	36 g	36 g	36 g
PEGDA	4 g	4 g	4 g	4 g	4 g
LAP	4 mg	4 mg	4 mg	4 mg	4 mg
Y/N ratio	0:1	1:60	1:25	1:10	1:0
cell loading	0 wt %	0.8 wt%	1.7 wt%	4.0 wt%	42.8 wt%
# of cells per cc	0	1.6×10^{8}	3.4×10^{8}	8.0×10^{8}	8.6×10^{9}
cell vol. density	0	1.4 vol%	2.9 vol%	7.0 vol%	75 vol%

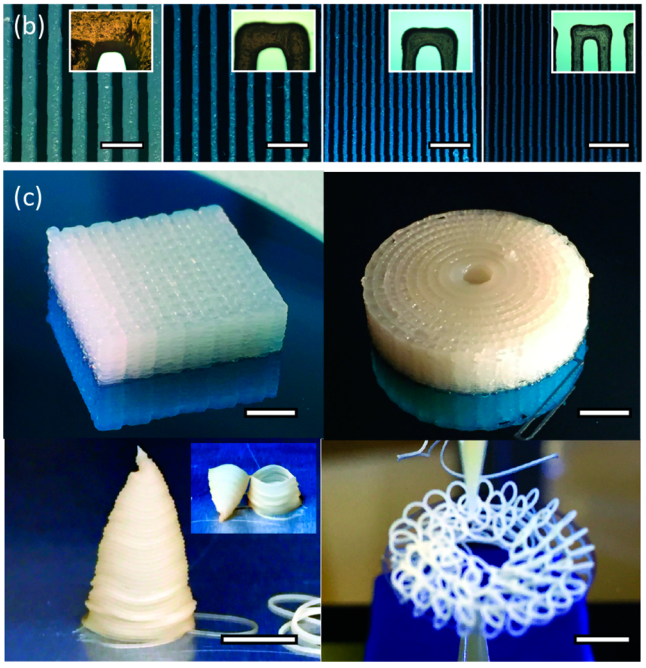

Figure 2. Representative inks with unique appearance and complex 3D-printed geometries. (a) Table comparing five ink compositions with increased cell loadings and photographs of various hand-molded geometries. (b) Two-dimensional serpentine patterns printed on a silicon wafer. Line thicknesses are increased. Scale bars are 5 mm. (c) Photographs taken from printed structures with increasing complexities. Scale bars are 5 mm.

yeast ink) is estimated to be 8.6×10^{9} cells/mL, or a volumetric ratio of 75 vol %. This cell concentration is significantly higher than a liquid culture of yeast cells grown under similar batch conditions where the typical cell density is ~10^{7} cells/mL (or 0.05 vol %).[15,16] Figure 2a also displays the composition of five representative ink compositions and various geometries of ink "doughs" molded by hand. Rather than appearing as viscous liquid/gels as conventional bioinks, these inks have solid shapes, yet liquefied in the presence of shear stress when extruded from a nozzle. This observation indicate they are viscoelastic materials with well-suited rheological behavior and shear-thinning properties.

A general challenge for extrusion-based printing is to tailor ink composition to achieve required rheology for reliable flow through fine nozzles and shape integrity after deposition. For inks that use a solid filler to tune rheology, the loading plays a key role in determining the printability: if the loading is too low, the printed shape is too soft to maintain the geometry; if the loading is too high, the ink can be too stiff to be extruded. To obtain comprehensive knowledge of this new ink type with dual solid fillers, we conducted systematic studies of ink rheology as a function of loading and ratio of the two fillers (Figure S2). We found nanocellulose inks were printable when loading is between ~10 and 40 wt %. Adding nanocellulose causes the inks plateau modulus (G_{eq}') to increase drastically from only ~3500 (15 wt %) to over 60 000 Pa elastic (35 wt %). Meanwhile, the 35 wt % ink showed an order of magnitude higher apparent viscosity than that of the 15 wt % ink. On the other hand, pure yeast inks are printable when the loading is between ~30 and 50 wt %. Similarly, when the cell concentration was increased from 35 to 50 wt %, the inks G_{eq}' displayed a dramatic increase from ~400 to ~40 000 Pa, while their shear flow curves exhibited almost the same negative slopes. These rheological values confirm that both cell and nanocellulose fillers can act as a viscosifier to generate a liquid-to-solid transition by imparting a yield stress to the precursor suspension. Because each component yielded inks with excellent shear-thinning behavior, the composite ink showed a full spectrum of printability with almost arbitrary yeast to nanocellulose ratio (Y/N ratio). For example, keeping the total solid loading at ~33 wt % while tuning the Y/N ratio from 1:0 to 0:1, the G_{eq}' of the composite inks varied across three orders of magnitude as the Y/N ratio changed. All composite inks showed strong thixotropic properties as their apparent viscosities decreased with shear rates. The magnitudes of the key rheological parameters of the ink presented here are in good agreement with those reported for other soft biomaterial-based inks designed for this 3D filamentary printing technique such as hydrogels ($G_{eq}' \approx 100-3000$ Pa; $\eta_0 \approx 200-5000$ Pa s),[17,18] silk fibroins ($G_{eq}' \approx 1$ Pa; $\eta_0 \approx 3$ Pa s),[19] cellulose nanocrystals ($G_{eq}' \approx 300\,000$ Pa; $\eta_0 \approx 100\,000$ Pa s),[20] and copolymers ($G_{eq}' \approx 10\,000$ Pa; $\eta_0 \approx 2000$ Pa s).[12,13,21] Taken together, this unique dual-filler formula allows us to prepare bioinks with tunable cell densities, mechanical stiffness, and rheological properties over a wide range.

To determine the printing resolution, we first printed two-dimensional serpentine patterns with decreasing nozzle sizes. Figure 2b shows the picture and optical microscope images of the printing results through nozzle sizes of 1.6, 0.8, 0.5, and 0.2 mm, respectively. The printed filaments had uniform thicknesses across the whole pattern. We noticed inhomogeneous "flakes" and surface roughness in inks that contained nanocellulose. These "flakes" did not affect extrusion and upon further investigation were found to be microscale nanocellulose not fully hydrated. Figure 2c displayed printed structures with increasing complexities. Microperiodic geometries of simple-cubic and cylindrical scaffolds were produced by repeated printing in-plane patterns while gradually lifting up the nozzle. Having excellent rheological properties, our inks allowed the creation of unconventional architectures, such as a hollow cone or a circular translating coil structure, assisted by viscous thread instability effect.[22] These latter architectures confirmed our inks had ultrahigh tensile strength and excellent self-supporting properties for manufacturing of intricate architectures.

DOI: 10.1021/acs.nanolett.9b00066
Nano Lett. 2019, 19, 5829−5835

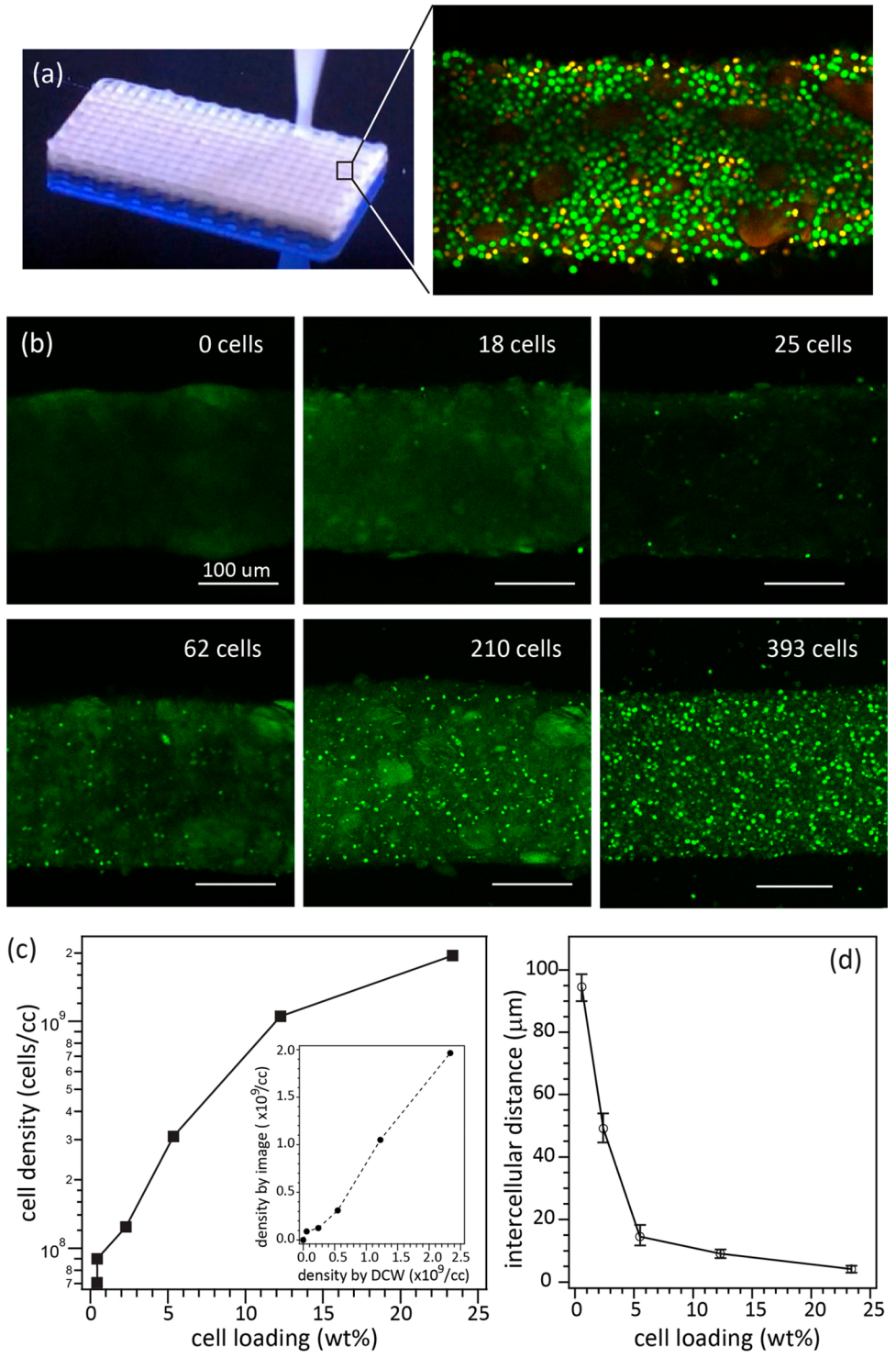

Figure 3. Cell viability assays and control of cell densities. (a) Live−dead stain of a 200-μm-thick single-filament from a printed lattice. (b) Confocal images taken from printed scaffolds of cell loadings of 0, 0.6, 2.4, 5.5, 12.3, and 23.4 wt %, respectively. Counted cell number per image is displayed. Scale bars are 100 μm. (c) Calculated cell densities from confocal images as a function of cell loading. Inset: plot of cell densities calculated from confocal images relative to those calculated from dry cell weight. (d) Averaged intercellular distance measured from each image and plotted versus cell loading.

The biocompatibility of ink composition and fabrication process was examined by live/dead cell viability assays and fluorescent confocal microscopy. As shown in Figure S3, we found cell viability in a cured lattice and in cell suspension were similar (31.4% and 35.9%, respectively), suggesting cell viability was determined by the original yeast granules used[23] rather than ink preparation and fabrication. Consistent with the observation of inhomogeneity under an optical microscope, patches with variable sizes of several tens microns were observed inside the filament (Figure 3a, dark red patches). These patches did not contain cells and were believed to be nanocellulose segregates. The impact of ink composition on

DOI: 10.1021/acs.nanolett.9b00066
Nano Lett. 2019, 19, 5829−5835

cell viability was studied on two distinct ink compositions, 5.5 and 23.4 wt % of cells (Figure S3, Video 2); in both case, cells were viable and uniformly dispersed in the three dimensions.

Tuning the cell loading during ink preparation allows rational control over cell densities and intercellular distance. Figure 3b compared laser-scanning confocal images taken from six representative filaments of increasing cell loading of 0, 0.6, 2.4, 5.5,12.3, 23.4 wt %, and decreasing nanocellulose loading of 28.6, 28.2, 26.8, 24.6, 19.7, 11.6 wt %, respectively. Quantitative image analysis revealed 0, 18, 25, 62, 210 to 393 individual cells per image, respectively. Figure 3c shows calculated cell densities from image analysis as a function of cell loading. Increasing cell loading in the ink yielded a linear increase in cell density as expected, and this curve can be used to calculate the dry cell weight (DCW) needed to prepare an ink for a desired cell density. Correlation of cell densities calculated from image analysis and those from DCW shows a linear correlation (Figure 3c, inset), and cell density calculated from image analysis was slightly lower than that estimated from DCW. This is because PEGDA-based hydrogels expand in volume after they are fully hydrated.[24] Lastly, together with the increase of cell loading/cell densities in the ink, intercellular distance drastically decreases accordingly (Figure 3d). In the 23.4 wt % cell loading sample, the calculated cell density from the image is 1.9×10^9 cells/cm^3, and the cell-to-cell distance was reduced to 4.3 μm, approaching the single-cell length scale.

At high cell densities, rapid delivery of nutrients and removal of metabolic waste are indispensable for good biocatalytic performance. In this regard, printed porous geometries can substantially enhance mass-transfer efficiency. It is well-known yeast cells ferment glucose into ethanol and CO_2 according to the following equation:

$$C_6H_{12}O_6 \text{ (glucose)} \rightarrow 2C_3H_4O_3 \text{ (pyruvate)} \rightarrow 2C_2H_5OH + 2CO_2\uparrow$$

To quantitatively study how geometry impacts catalytic activity of live cells, we prepared porous lattices and solid layers using the same ink material. Several identical lattices were printed having a nominal area of 1 cm^2, a thickness of ~1.5 mm, and 200 μm filament resolution. Meanwhile, bulk samples made of the same ink were prepared by photocuring a film of the same thickness and area. Each sample was weighed prior to immersion in medium for subsequent normalization of their catalytic performance. Figure 4a compares pictures of bulk and printed lattices immersed in YPD media at different time points. In both cases, within a minute after submersion in fresh YPD medium, CO_2 gas bubbles were generated and released from the surface of hydrogels. Interestingly, CO_2 was released much faster from the lattices than from the bulk film counterparts (Video 3). As a result, after several minutes of incubation, bulk films floated up, while lattices remained submerged in the medium. We attribute this phenomenon to efficient mass transfer in printed lattices due to structural porosity as well as thin filaments, both leading to enhanced surface area at the hydrogel/medium interface, where the exchange of the nutrients, products, and gas is enhanced. Once CO_2 is generated from the cells, it is rapidly diffused through the filament and released into the medium. However, for bulk films, the average diffusion length of CO_2 inside the material is substantially larger than the thin filament of lattices and gas

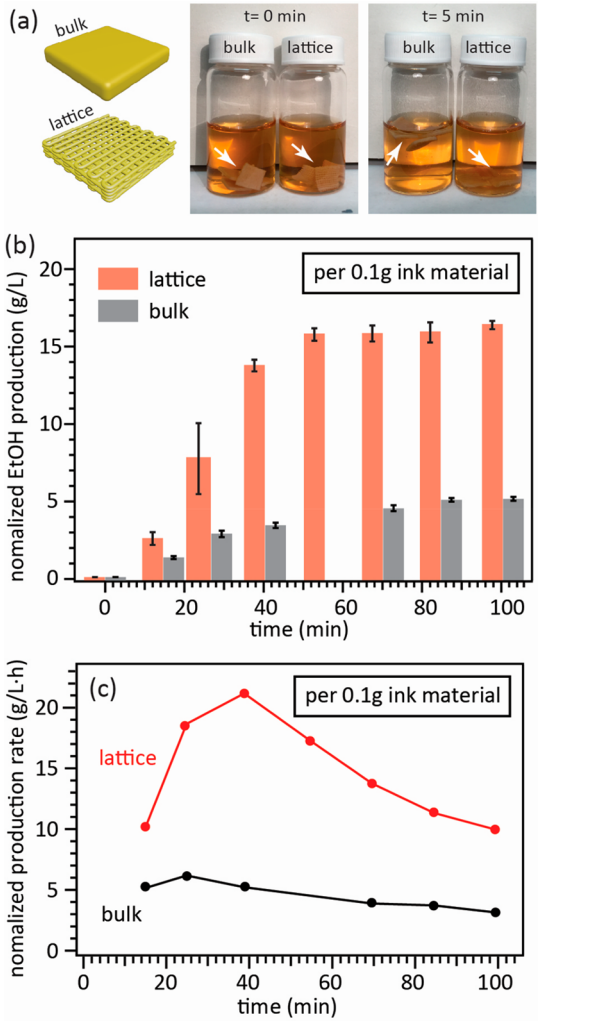

Figure 4. Ethanol production from encapsulated live cells. (a) Left: schematic of a solid film and a printed lattice of living materials. Right: photographs of two vials containing solid films and printed lattices, immediately after immersion into medium and after 5 min incubation in the medium. White arrows highlighted the location of the samples. (b) Normalized volumetric productivity of ethanol from lattices (red) and bulk hydrogels (gray). (c) Normalized ethanol production rate of lattice (red) and bulk hydrogels (black) as a function of time.

diffusion is slow. As a result, gas bubbles were trapped inside and caused the samples to float up in the medium. Quantitative measurements of ethanol production made by gas chromatography were consistent with this observation. Ethanol production from printed lattices and bulk films, normalized by the weight of the bioink used, is shown in Figure 4b. After a short lag period, both structures produced ethanol. The printed lattices rapidly produced ethanol and the reaction reached completion in less than an hour due to glucose depletion, which was also coincident with a decrease in CO_2 generation. At the end of the reaction, the lattices, on average, generated 16.1 g/L ethanol per 0.1 g ink material, and the final concentration in the spent medium was ~3.7 v/v %. In the meanwhile, bulk film samples produced merely 5.1 g/L ethanol per 0.1 ink material, less than one-third of the lattice production (Figure 4b). We attribute this to the poor mass transfer in bulk hydrogels that limits access to glucose and causes metabolic waste accumulation, negatively impacting the culture microenvironment. In terms of reaction rate, ethanol

DOI: 10.1021/acs.nanolett.9b00066
Nano Lett. 2019, 19, 5829−5835

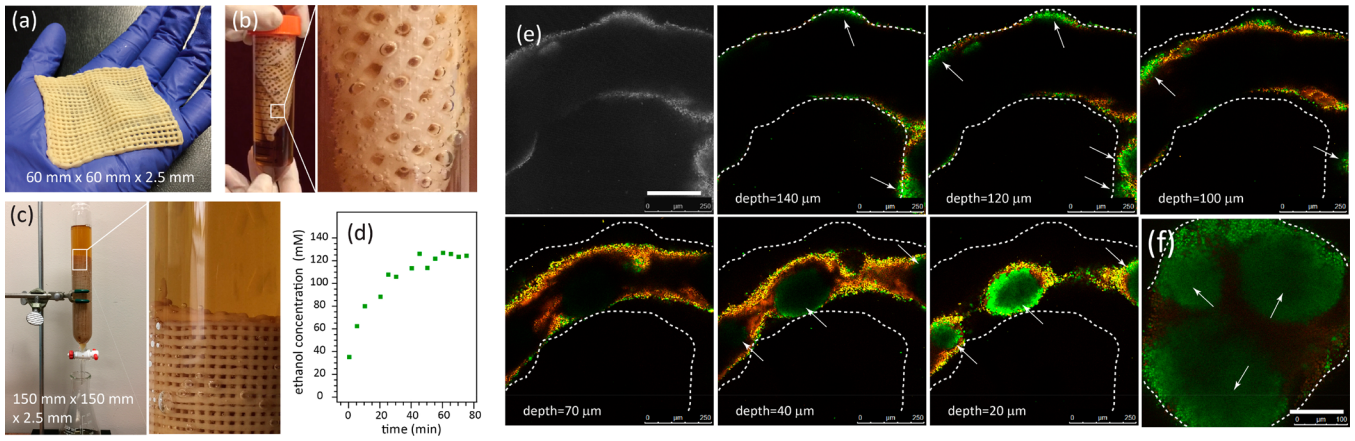

Figure 5. Large-scale bioprinting and long-term culture. (a) Photograph of a palm-size lattice. (b) Photographs of the same lattice soaked in medium in a falcon tube. (c) Photograph of a 225 cm^2 lattice rolled up in a GC column and (d) its ethanol production after 2 weeks. (e) Bright-field and confocal images of a filament from a one-month-old lattice. Scale bar is 200 μm. White dotted lines indicate the edge of the filament. Arrows indicate the position of live colonies. (f) Cross-sectional confocal image taken from the same sample. Scale bar is 100 μm.

produced by the lattices was up to 21 g ethanol/L h, while the bulk films merely had a productivity of 5 g ethanol/L h (Figure 4c). Taken together, these results suggest the ability to design and print optimized 3D geometries can improve mass exchange at the hydrogel/medium interface resulting in high catalytic efficiency.

Practical applications using catalytic microorganisms are usually performed in pilot-scale stirred-tank reactors for producing large quantities of products. To demonstrate the potential of 3D printed cell to be integrated with existing large-scale industrial infrastructure, we increased the printing dimensions and studied the lifetime of printed cells. Figure 5a shows a palm-sized lattice mat with an area of 36 cm^2. The mat was then rolled up to fit into a 50-mL falcon tube and immersed in YPD medium with the cap closed. As shown in Figure 5b and Video 4, CO_2 bubbles were rapidly generated and the medium was carbonated. As a result, upon opening the cap, the dissolved CO_2 was released and liquid overflowed (Video 5). We further increased the printing scale to 225 cm^2. The mat was then inserted into a chromatography column, a configuration that could be leveraged for both batch and continuous-flow operations (Figure 5c). This scaffold was incubated at room temperature and fed every other day. Ethanol production measured after 2 weeks is shown in Figure 5d. Upon medium replenishment, the ethanol concentration increased within an hour, consistent with the visual observation of CO_2 generation (Video 6). The final ethanol concentration in the medium was detected as ~120 mM, corresponding to a 0.7 v/v % of ethanol. The ethanol yield is lower than the value achieved in small-scale lattices (3.7 v/v%), potentially due to cell aging. Synergistic optimization of scaffold geometry, bioreactor design, and culture conditions are needed to improve the reactor performance when scaled.

Lastly, we examined the cell viability and spatial distribution in a lattice that has been cultured for a month with confirmed glucose fermentation activity. A series of confocal images taken at different imaging depths of a section of 200-μm filament are shown in Figure 5e. Compared to a freshly printed scaffolds featuring a smooth filament surface and uniform cell distribution (Figure 3), the filament surface became bumpy after a month of incubation (Figure 5e), which indicated a change in the biomaterial homogeneity. Confocal microscope images with live−dead staining showed that the bumps consisted of live cell colonies, with an average size of 100−200 μm, still encapsulated in the hydrogel (Figure 5e). Figure 5f showed the cross-sectional confocal image of a single filament in which at least three live colonies were clearly observed. We also note that in addition to yeast cells with a characteristic 4-μm spherical shape, there was an indication of 1-μm length, rod-shaped bacterial cells (Figure S4). These bacterial cells appeared only on the filament surface yet not penetrating it, which suggested that hydrogels may provide protection of yeast cells from bacterial contaminants. Cultured under a nonoptimized, nonsterile condition for 4 months, the printed scaffold still generated CO_2 gas immediately after the addition of fresh medium (Video 7). These observations provide new insights into the long-term culture of printed living materials as biocatalysts.

In summary, we developed a new bioink material that enabled additive manufacturing of self-supporting 3D geometries with high resolution, large scale, and high cell density. With an unprecedented cell loading, we discovered that the cells exerted substantial impact on ink rheology, and the cell inks had shear-thinning behavior desired for extrusion-based printing. By using a secondary shear-thinning filler of nanocellulose, we were able to tune the cell density and intercellular distance down to single-cell level. Printed cells produced CO_2 gas and ethanol from glucose fermentation, as evidenced by gas bubble generation as well as detection of ethanol in the medium. Compared to bulk film counterparts, printed lattices with thin filament and macro-pores allowed rapid mass-transfer leading to several-fold increase in ethanol generation. Although Baker's yeast used in this work is optimized for gas generation, genetically modified yeast cells can produce pharmaceuticals, chemicals, food, and biofuels, which are highly valuable products.[25−28] Our ink system can be applied to a variety of other catalytic microbes to address broad application needs. The ability to print live whole cells into mass-transfer efficient 3D geometries will be meaningful toward industrial biosynthesis of valuable product with engineered cells and intensification of such bioprocesses.

DOI: 10.1021/acs.nanolett.9b00066
Nano Lett. 2019, 19, 5829−5835

■ ASSOCIATED CONTENT

Supporting Information

The Supporting Information is available free of charge on the ACS Publications website at DOI: 10.1021/acs.nanolett.9b00066.

Ink preparation method, rheology test, printing process, confocal fluorescent imaging measurement and results (PDF)

Video of real-time printing (MPG)

Video of ink composition impact on cell viability (MPG)

Video of CO_2 release from lattice (MPG)

Video of CO_2 bubbles rapidly generated and the medium carbonized (MPG)

Video of cap opening: dissolved CO_2 was released and liquid overflowed (MPG)

Video of ethanol concentration increase upon medium replenishment (MPG)

Video of printed scaffold generated CO_2 gas immediately after addition of fresh medium on day 142 (MPG)

■ AUTHOR INFORMATION

Corresponding Authors

*E-mail: qian3@llnl.gov.

*E-mail: baker74@llnl.gov.

ORCID

Fang Qian: 0000-0002-8782-4285

Jennifer M. Knipe: 0000-0001-9544-0444

Notes

The authors declare no competing financial interest.

■ ACKNOWLEDGMENTS

The authors thank Dr. Congwang Ye for providing nanocellulose crystal powder, Drs. Michael Grapes and Max Murialdo for training on the Hyrel printer, and Charlene Li for monitoring gas bubble generation. This work was supported by Lawrence Livermore National Laboratory under the auspices of the U.S. Department of Energy under Contract No. DE-AC52-07NA27344, through LDRD Award No. 17-FS-027 and 19-ERD-005. The IM release number of the manuscript is LLNL-JRNL-753559.

■ REFERENCES

(1) Murphy, S. V.; Atala, A. *Nat. Biotechnol.* **2014**, *32*, 773−785.

(2) Kolesky, D. B.; Homan, K. A.; Skylar-Scott, M. A.; Lewis, J. A. *Proc. Natl. Acad. Sci. U. S. A.* **2016**, *113* (12), 3179−84.

(3) Gu, Q.; Tomaskovic-Crook, E.; Wallace, G. G.; Crook, J. M. *Adv. Healthcare Mater.* **2017**, *6* (17), 1700175.

(4) Espinosa-Hoyos, D.; Jagielska, A.; Homan, K. A.; Du, H.; Busbee, T.; Anderson, D. G.; Fang, N. X.; Lewis, J. A.; Van Vliet, K. J. *Sci. Rep.* **2018**, *8* (1), 478.

(5) Laronda, M. M.; Rutz, A. L.; Xiao, S.; Whelan, K. A.; Duncan, F. E.; Roth, E. W.; Woodruff, T. K.; Shah, R. N. *Nat. Commun.* **2017**, *8*, 15261.

(6) Knowlton, S.; Onal, S.; Yu, C. H.; Zhao, J. J.; Tasoglu, S. *Trends Biotechnol.* **2015**, *33* (9), 504−13.

(7) Zhang, Y. S.; Duchamp, M.; Oklu, R.; Ellisen, L. W.; Langer, R.; Khademhosseini, A. *ACS Biomater. Sci. Eng.* **2016**, *2* (10), 1710−1721.

(8) Varma, A.; Podila, G. K. *Biotechnological Applications of Microbes*; Anshan, 2006.

(9) McNeil, B.; Archer, D.; Giavasis, I.; Harvey, L. *Microbial Production of Food Ingredients, Enzymes and Nutraceuticals*; Elsevier, 2013.

(10) Lehner, B. A. E.; Schmieden, D. T.; Meyer, A. S. *ACS Synth. Biol.* **2017**, *6* (7), 1124−1130.

(11) Schaffner, M.; Ruhs, P. A.; Coulter, F.; Kilcher, S.; Studart, A. R. *Science advances* **2017**, *3* (12), No. eaao6804.

(12) Liu, X.; Yuk, H.; Lin, S.; Parada, G. A.; Tang, T. C.; Tham, E.; de la Fuente-Nunez, C.; Lu, T. K.; Zhao, X. *Adv. Mater.* **2018**, *30* (4), 1870021.

(13) Saha, A.; Johnston, T. G.; Shafranek, R. T.; Goodman, C. J.; Zalatan, J. G.; Storti, D. W.; Ganter, M. A.; Nelson, A. *ACS Appl. Mater. Interfaces* **2018**, *10* (16), 13373−13380.

(14) Sabnis, A.; Rahimi, M.; Chapman, C.; Nguyen, K. T. *J. Biomed. Mater. Res., Part A* **2009**, *91* (1), 52−9.

(15) *Useful Fundamental Numbers in Molecular Biology*; BioNumbers, 2018. http://kirschner.med.harvard.edu/files/bionumbers/fundamentalBioNumbersHandout.pdf.

(16) Mahazar, N. H.; Zakuan, Z.; Norhayati, H.; MeorHussin, A. S.; Rukayadi, Y. *Pak. J. Biol. Sci.* **2017**, *20*, 154−159.

(17) Hanson Shepherd, J. N.; Parker, S. T.; Shepherd, R. F.; Gillette, M. U.; Lewis, J. A.; Nuzzo, R. G. *Adv. Funct. Mater.* **2011**, *21* (1), 47−54.

(18) Barry, R. A., III; Shepherd, R. F.; Hanson, J. N.; Nuzzo, R. G.; Wiltzius, P.; Lewis, J. A. *Adv. Mater.* **2009**, *21*, 1−4.

(19) Ghosh, S.; Parker, S. T.; Wang, X.; Kaplan, D. L.; Lewis, J. A. *Adv. Funct. Mater.* **2008**, *18*, 1883−1889.

(20) Siqueira, G.; Kokkinis, D.; Libanori, R.; Hausmann, M. K.; Gladman, A. S.; Neels, A.; Tingaut, P.; Zimmermann, T.; Lewis, J. A.; Studart, A. R. *Adv. Funct. Mater.* **2017**, *27*, 1604619.

(21) Kolesky, D. B.; Truby, R. L.; Gladman, A. S.; Busbee, T. A.; Homan, K. A.; Lewis, J. A. *Adv. Mater.* **2014**, *26* (19), 3124−30.

(22) Passieux, R.; Guthrie, L.; Rad, S. H.; Levesque, M.; Therriault, D.; Gosselin, F. P. *Adv. Mater.* **2015**, *27* (24), 3676−80.

(23) N'Guessan, F. K.; Coulibaly, H. W.; Alloue-Boraud, M. W.; Cot, M.; Dje, K. M. *Food Sci. Nutr.* **2016**, *4* (1), 34−41.

(24) Cavallo, A.; Madaghiele, M.; Masullo, U.; Lionetto, M. G.; Sannino, A. *J. Appl. Polym. Sci.* **2017**, *134*, 4438021.

(25) Liu, X.; Cheng, J.; Zhang, G.; Ding, W.; Duan, L.; Yang, J.; Kui, L.; Cheng, X.; Ruan, J.; Fan, W.; Chen, J.; Long, G.; Zhao, Y.; Cai, J.; Wang, W.; Ma, Y.; Dong, Y.; Yang, S.; Jiang, H. *Nat. Commun.* **2018**, *9*, 448.

(26) Li, Y.; Li, S.; Thodey, K.; Trenchard, I.; Cravens, A.; Smolke, C. D. *Proc. Natl. Acad. Sci. U. S. A.* **2018**, *115*, E3922−3931.

(27) Branduardi, P.; Smeraldi, C.; Porro, D. *Mol. Microbiol. Biotechnol.* **2008**, *15*, 31−40.

(28) Denby, C. M.; Li, R. A.; Vu, V. T.; Costello, Z.; Lin, W.; Chan, L. J. G.; Williams, J.; Donaldson, B.; Bamforth, C. W.; Petzold, C. J.; Scheller, H. V.; Martin, H. G.; Keasling, J. D. *Nat. Commun.* **2018**, *9*, 965.

DOI: 10.1021/acs.nanolett.9b00066
Nano Lett. 2019, 19, 5829−5835